

Constraints on a 2HDM with a singlet scalar and implications in the search for heavy bosons at the LHC

Stefan von Buddenbrock,¹ Alan S. Cornell,¹ Elie D. R. Iarilala,¹ Mukesh Kumar,¹ Bruce Mellado,^{1,2}, Xifeng Ruan¹ and Esra Mohammed Shrif¹

¹School of Physics and Institute for Collider Particle Physics, University of the Witwatersrand, Johannesburg, Wits 2050, South Africa.

²iThemba LABS, National Research Foundation, PO Box 722, Somerset West 7129, South Africa.

E-mail: stef.von.b@cern.ch, alan.stanley.cornell@cern.ch, iarilala@aims.ac.za, mukesh.kumar@cern.ch, bmellado@mail.cern.ch, xifeng.ruan@cern.ch, esra.mohammed.shrif@cern.ch

Abstract. We study a two-Higgs doublet model extended with an additional singlet scalar (2HDM+S), and provide a brief introduction to the model and its parameters. Constraints are applied to the parameter space of this model in order to accommodate a number of features in the data that have been interpreted in Ref. [1] as the result of the $H \rightarrow Sh$ decay produced via gluon-gluon fusion and in association with top quarks. Implications on the phenomenology of the heavy pseudo-scalar (A) and charged scalar (H^\pm) are discussed. In particular, the decays $A \rightarrow ZH$ and $H^\pm \rightarrow W^\pm H$ become prominent. This leads to final states with multiple leptons and b -quarks. The decay $A \rightarrow ZH \rightarrow ZSh$ results in the production of a high transverse momentum Z produced in association with a lepton and two b -quarks with little additional jet activity. These predictions are compared to the data with model's benchmark points. With the parameters obtained here the model is able to accommodate the features at the LHC reported in Ref. [1]. Without varying these parameters additional excesses in the $Zb\bar{b}$ and $t\bar{t}$ invariant mass spectra, and the production of 3 leptons plus two b -tagged jets can be explained assuming $m_A \approx 600$ GeV.

Submitted to: *J. Phys. G: Nucl. Part. Phys.*

Keywords: Higgs boson, singlet scalar, heavy scalar, multiple leptons

1. Introduction

The discovery of a Higgs boson [2–5] at the Large Hadron Collider (LHC) [6, 7] represents a new window of opportunity for the field of particle physics. Following this discovery, the focus has shifted towards the understanding of the couplings of this boson to particles in the Standard Model (SM) and beyond (BSM), and towards the search for new bosons. The Run 2 at the LHC is expected to deliver about 140 fb^{-1} of usable data at a proton-proton centre of mass energy of 13 TeV. Most of the studies released by the experiments at the LHC have been

performed on a quarter of this data set. Furthermore, some important studies have not yet been released with Run 2 data altogether.

In Refs. [8–10] the scalars H and S were introduced via an effective model to explain a number of features in the Run 1 data. These include distortions of the Higgs boson transverse momentum spectrum, accompanied with elevated associated jet activity, elevated rates of leptons in association with b -tagged jets used for the search of the associated production of the Higgs boson with top quarks, and results from the search for double Higgs boson and weak boson production. The potential impact on the measurements of some of the signal strengths of the newly discovered Higgs boson has been evaluated in Ref. [11]. The relevance and advantages of electron-proton collisions to search for additional scalar bosons has also been pointed out in Refs. [12–14].

Simple extensions of the Standard Model (SM) are the two-Higgs doublet models (2HDMs) [15, 16], which need an additional Higgs-doublet in the model. As a result of this additional doublet, the scalar spectrum is populated with two CP-even (h, H), one CP-odd (A) and charged (H^\pm) scalar bosons.[‡] Note that 2HDMs have been explored in the literature, where various facets related to the theory, phenomenology and constraints on these models using the experimental data from different collider environments have been explored [16, 17] (and refs. therein). However, as pointed out in Refs. [9, 10, 18, 19], a 2HDM alone is not able to accommodate the above-mentioned features of the data. As a result, a scalar singlet S is introduced in conjunction with a 2HDM in Ref. [10], referred to here as the 2HDM+S model. In addition, this type of model may also be able to explore scenarios with dark matter. In Ref. [10] it was discussed that a 2HDM+S model would result in the anomalous production of multiple leptons. This hypothesis has been compared to data [1, 20], where large discrepancies between the data and SM Monte Carlos are observed that cannot be resolved with the current understanding of theoretical systematics. The features of the data examined in Ref. [1] have been studied with additional data in Ref. [21]. This study indicates that these features have become more pronounced with more data.

Here we expand on the phenomenology described in Ref. [1, 10]. Firstly in this paper we identify the parameter space of the 2HDM+S model that accommodates the features in the data studied in Ref. [1]. Secondly, here we also evaluate the implications of this choice of parameter space for the heavy pseudo-scalar and the charged scalar. We are particularly interested in investigating the CP-odd scalar in the 2HDM+S model. In particular, we study the production of A through the gluon-gluon-fusion (ggF) mode, and its decay into $A \rightarrow ZH$ channels, where the decay modes $H \rightarrow hh, Sh, SS$ are considered. This setup leads to a number of interesting final states with leptons and b -tagged jets.

The resulting kinematics of the decay of $A \rightarrow ZH$, where $m_A > m_Z + m_H$ and $H \rightarrow SS, Sh$, have been studied in Ref. [10]. Assuming that the width of A is much smaller than the experimental resolution obtained with the $l\bar{l}b\bar{b}$ decay, it was noted that a relatively narrow structure in the invariant mass spectrum of Zh is expected, such that $m_{Zh} < m_A$.

A structure in the Zh invariant mass spectrum has been reported by the ATLAS

[‡] Here we consider h as the lighter Higgs boson as in the SM with $m_h = 125$ GeV.

collaboration [22] with Run 2 data. The CMS collaboration has reported limits with Run 1 and Run 2 data that do not contradict the aforementioned results [23, 24]. The structure has been interpreted in terms of the decay $A \rightarrow Zh$ within a 2HDM, with a cross-section $\sigma(pp \rightarrow Zh) \approx 100 - 300 \text{ fb}$ in Ref. [25]. Here we interpret the structure in terms of the 2HDM+S model with the spectroscopy discussed in Refs. [8, 10] and Ref. [1], where $m_H \approx 270 \text{ GeV}$ and $m_S \approx 150 \text{ GeV}$. The structure includes events with more than two b -tagged jets, which can be interpreted within a 2HDM as coming from a bottom-quark induced production of the CP-odd boson at intermediate values of $\tan\beta$. Here the production of Zh with additional b -tagged jets from $A \rightarrow ZH \rightarrow ZSh, Zhh$ is discussed.

Note also that the CMS collaboration has reported discrepancies of 2.85σ in the production of three leptons, where one pair comes from the decay of a Z boson, in association with b -tagged jets but with reduced hadronic jet activity [26, 27]. These events are identified in the context of studying ttZ production where the discrepancy emerges with low jet multiplicity. This excess can be explained by the production $A(600) \rightarrow ZH(270) \rightarrow ZS(145)h, Zhh$. In this setup we elaborate on the resulting characteristics corresponding to the production of three leptons, including a Z boson in association with b -tagged jets. The potential impact of the signal from a heavy CP-odd boson discussed in Ref. [25] is considered here on the measurement of the signal strength of Vh , ($V = ZW$) production.

This paper is organised into the following sections: In section 2 we describe the model, in section 3 we describe the tools used and constraints imposed on the parameter scan, reporting on the allowed region of the parameter space where the implications on the branching ratios of the heavy pseudo-scalar and charged scalar are reported. In section 4 the findings from section 3 are compared to the data, and in section 5 we summarise and conclude.

2. The Model

Following Ref. [10, 28, 29], a 2HDM with an additional real singlet Φ_S is the baseline for our formalism, where we use the notation used in Ref. [28], and call this model the 2HDM+S. As such, the potential is given by:

$$\begin{aligned} V(\Phi_1, \Phi_2, \Phi_S) = & m_{11}^2 |\Phi_1|^2 + m_{22}^2 |\Phi_2|^2 - m_{12}^2 (\Phi_1^\dagger \Phi_2 + \text{h.c.}) + \frac{\lambda_1}{2} (\Phi_1^\dagger \Phi_1)^2 + \frac{\lambda_2}{2} (\Phi_2^\dagger \Phi_2)^2 \\ & + \lambda_3 (\Phi_1^\dagger \Phi_1) (\Phi_2^\dagger \Phi_2) + \lambda_4 (\Phi_1^\dagger \Phi_2) (\Phi_2^\dagger \Phi_1) + \frac{\lambda_5}{2} \left[(\Phi_1^\dagger \Phi_2)^2 + \text{h.c.} \right] \\ & + \frac{1}{2} m_S^2 \Phi_S^2 + \frac{\lambda_6}{8} \Phi_S^4 + \frac{\lambda_7}{2} (\Phi_1^\dagger \Phi_1) \Phi_S^2 + \frac{\lambda_8}{2} (\Phi_2^\dagger \Phi_2) \Phi_S^2. \end{aligned} \quad (1)$$

Here the fields Φ_1 and Φ_2 are the $SU(2)_L$ Higgs doublets. The first two lines are the terms from real 2HDM potential, while the last line contains the contribution of the singlet field Φ_S . Generally, models with more than one Higgs doublet have tree-level Flavour Changing Neutral Currents (FCNC). To prevent tree-level FCNCs, we must couple all quarks of a given charge to a single Higgs doublet. This can be accomplished by imposing a \mathbb{Z}_2 symmetry, which can be softly broken by the term m_{12}^2 . Also, the extension of the \mathbb{Z}_2 symmetry to the

Yukawa sector guarantees the absence of FCNC at tree-level. A trivial generalisation of the usual 2HDM \mathbb{Z}_2 symmetry requires:

$$\Phi_1 \longrightarrow \Phi_1, \quad \Phi_2 \longrightarrow -\Phi_2, \quad \Phi_S \longrightarrow \Phi_S. \quad (2)$$

One can also consider another \mathbb{Z}'_2 symmetry:

$$\Phi_1 \longrightarrow \Phi_1, \quad \Phi_2 \longrightarrow \Phi_2, \quad \Phi_S \longrightarrow -\Phi_S, \quad (3)$$

which is not broken explicitly. For our study, we consider a scenario where the real singlet field Φ_S acquires a vacuum expectation value (v_{ev}) with \mathbb{Z}_2 symmetry.[§] Note that if Φ_S doesn't acquire a v_{ev} , the \mathbb{Z}'_2 symmetry then becomes a source of a viable dark matter candidate.

In this work we set the term $m_{12}^2 \neq 0$ in the 2HDM+S potential, which corresponds to a soft breaking of the \mathbb{Z}_2 symmetry, and consider the λ_i to be real, which corresponds to a model without explicit CP violation. More discussions can be found in Refs. [28, 30, 31].

Assuming the v_{ev} s for the fields $\Phi_1 \rightarrow v_1/\sqrt{2}$, $\Phi_2 \rightarrow v_2/\sqrt{2}$ and $\Phi_S \rightarrow v_S$ are real after electroweak symmetry breaking (EWSB), the minimisation of the potential of the three Higgs fields leads to the three minimisation conditions:

$$\frac{\partial V}{\partial v_1} = \frac{\partial V}{\partial v_2} = \frac{\partial V}{\partial v_S} = 0. \quad (4)$$

The first derivative conditions for Φ_i ($i = 1, 2, S$) are:

$$\frac{\partial V}{\partial \Phi_1} = 0 \rightarrow m_{11}^2 = -\frac{1}{2}(v_1^2 \lambda_1 + v_2^2 \lambda_{345} + v_S^2 \lambda_7) + \frac{v_2}{v_1} m_{12}^2, \quad (5)$$

$$\frac{\partial V}{\partial \Phi_2} = 0 \rightarrow m_{22}^2 = -\frac{1}{2}(v_2^2 \lambda_2 + v_1^2 \lambda_{345} + v_S^2 \lambda_8) + \frac{v_2}{v_1} m_{12}^2, \quad (6)$$

$$\frac{\partial V}{\partial \Phi_S} = 0 \rightarrow m_S^2 = -\frac{1}{2}(v_1^2 \lambda_7 + v_2^2 \lambda_8 + v_S^2 \lambda_6), \quad (7)$$

where $\lambda_{345} \equiv \lambda_3 + \lambda_4 + \lambda_5$. Further, the doublet fields Φ_1 , Φ_2 and singlet field Φ_S can be parameterised as:

$$\Phi_1 = \begin{pmatrix} \phi_1^\pm \\ \frac{1}{\sqrt{2}}(v_1 + \rho_1 + i\eta_1) \end{pmatrix}, \quad \Phi_2 = \begin{pmatrix} \phi_2^\pm \\ \frac{1}{\sqrt{2}}(v_2 + \rho_2 + i\eta_2) \end{pmatrix}, \quad \Phi_S = v_S + \rho_S, \quad (8)$$

where ϕ_j^\pm ($j = 1, 2$) are the charged complex fields, ρ_i are real neutral CP-even fields and η_i are the real CP-odd fields. By substituting the parametrisation (8) into the Higgs potential (1), the mass matrices in the gauge basis can be easily obtained from the second derivatives of the fields. Accordingly, the mass-matrix for the charged ($M_{H^\pm}^2$) and CP-odd (M_A^2) scalar sector will remain as it is in the 2HDM. Using a 2×2 rotation matrix, given as:

$$\begin{pmatrix} G^\pm \\ H^\pm \end{pmatrix} = \begin{pmatrix} \cos \beta & \sin \beta \\ -\sin \beta & \cos \beta \end{pmatrix} \begin{pmatrix} \phi_1^\pm \\ \phi_2^\pm \end{pmatrix}, \quad (9)$$

[§] In principle Φ_S could be a complex singlet, and, in this case, the discrete \mathbb{Z}_2 symmetry would be promoted to a global $U(1)$ symmetry, where the spontaneous breaking would lead to a massless pseudo-scalar. This might be important and acceptable for phenomenology if it does not couple to the SM particles [30].

where G^\pm are a pair of charged Goldstone bosons and H^\pm are the physical charged scalars; the mass squared charged scalar matrix is the same as in a 2HDM. It can be represented as:

$$M_{H^\pm}^2 = \begin{pmatrix} -(2m_{12}^2 + (\lambda_4 + \lambda_5)v_1v_2)\frac{v_2}{2v_1} & m_{12}^2 + \frac{1}{2}(\lambda_4 + \lambda_5)v_1v_2 \\ m_{12}^2 + \frac{1}{2}(\lambda_4 + \lambda_5)v_1v_2 & -(2m_{12}^2 + (\lambda_4 + \lambda_5)v_1v_2)\frac{v_2}{2v_1} \end{pmatrix}. \quad (10)$$

Similarly, the CP-odd scalar sector can be diagonalised using the same 2×2 rotation matrix:

$$\begin{pmatrix} G^0 \\ A \end{pmatrix} = \begin{pmatrix} \cos\beta & \sin\beta \\ -\sin\beta & \cos\beta \end{pmatrix} \begin{pmatrix} \eta_1 \\ \eta_2 \end{pmatrix}, \quad (11)$$

where G^0 is a neutral Goldstone boson, A is the physical pseudo-scalar, and $\eta_{1,2}$ are real CP-odd fields. The mass squared CP-odd scalar matrix is exactly the same as in the 2HDM. It can be formulated as:

$$M_A^2 = \begin{pmatrix} -(m_{12}^2 + \lambda_5v_1v_2)\frac{v_2}{v_1} & m_{12}^2 + \lambda_5v_1v_2 \\ m_{12}^2 + \lambda_5v_1v_2 & -(m_{12}^2 + \lambda_5v_1v_2)\frac{v_2}{v_1} \end{pmatrix}, \quad (12)$$

where diagonalising the CP-odd mass squared matrix will result in the pseudo-scalars physical mass eigenstates A .

Since the 2HDM+S CP-even Higgs sector consists of additional Higgs bosons with respect to the 2HDM, due to the addition of the real scalar singlet, the CP-even neutral Higgs mass matrix is enlarged to a 3×3 matrix. In the interaction basis, (ρ_1, ρ_2, ρ_3) , it can be written as (using eqs. (5)-(7)):

$$M_{\text{CP-even}}^2 = \begin{pmatrix} \lambda_1 c_\beta^2 v^2 + t_\beta m_{12}^2 & -m_{12}^2 + \lambda_{345} c_\beta s_\beta v^2 & \lambda_7 c_\beta v v_S \\ -m_{12}^2 + \lambda_{345} c_\beta s_\beta v^2 & \lambda_2 s_\beta^2 v^2 + m_{12}^2 / t_\beta & \lambda_8 s_\beta v v_S \\ \lambda_7 c_\beta v v_S & \lambda_8 s_\beta v v_S & \lambda_6 v_S^2 \end{pmatrix}, \quad (13)$$

and it can be diagonalised by an orthogonal 3×3 matrix \mathcal{R} , in terms of mixing angles α_k ($k = 1, 2, 3$), and given as:||

$$\mathcal{R} = \begin{pmatrix} c_{\alpha_1} c_{\alpha_2} & s_{\alpha_1} c_{\alpha_2} & s_{\alpha_2} \\ -(c_{\alpha_1} s_{\alpha_2} s_{\alpha_3} + s_{\alpha_1} c_{\alpha_3}) & c_{\alpha_1} c_{\alpha_3} - s_{\alpha_1} s_{\alpha_2} s_{\alpha_3} & c_{\alpha_2} s_{\alpha_3} \\ -c_{\alpha_1} s_{\alpha_2} c_{\alpha_3} + s_{\alpha_1} s_{\alpha_3} & -(c_{\alpha_1} s_{\alpha_3} + s_{\alpha_1} s_{\alpha_2} c_{\alpha_3}) & c_{\alpha_2} c_{\alpha_3} \end{pmatrix}. \quad (14)$$

The three physical mass eigenstates h, S and H in terms of the interaction basis (ρ_1, ρ_2, ρ_3) , are given as:

$$\begin{pmatrix} h \\ S \\ H \end{pmatrix} = \mathcal{R} \begin{pmatrix} \rho_1 \\ \rho_2 \\ \rho_S \end{pmatrix}. \quad (15)$$

|| The abbreviations used here are $s_{\alpha_k} \equiv \sin \alpha_k$, $c_{\alpha_k} \equiv \cos \alpha_k$ and $t_\beta \equiv \tan \beta$, where t_β is defined as $t_\beta = v_2/v_1$ and $v^2 = v_1^2 + v_2^2$. By letting $\alpha_{2,3} \rightarrow 0$ and $\alpha_1 \rightarrow \alpha + \pi/2$ the 2HDM+S approaches the limit of a 2HDM with an added decoupled singlet, where α diagonalises the 2×2 mass matrix of the CP-even sector.

	u -type	d -type	leptons
type I	\mathcal{R}_{i2}/s_β	\mathcal{R}_{i2}/s_β	\mathcal{R}_{i2}/s_β
type II	\mathcal{R}_{i2}/s_β	\mathcal{R}_{i1}/c_β	\mathcal{R}_{i1}/c_β
lepton-specific	\mathcal{R}_{i2}/s_β	\mathcal{R}_{i2}/s_β	\mathcal{R}_{i1}/c_β
flipped	\mathcal{R}_{i2}/s_β	\mathcal{R}_{i1}/c_β	\mathcal{R}_{i2}/s_β

Table 1. The coupling coefficient $c(H_i f f)$ as defined in eq. (19).

Here the mixing angles $\alpha_{1,2,3}$ for the CP-even Higgs states can be constrained within $-\pi/2 < \alpha_{1,2,3} < \pi/2$, without loss of generality. And thus the CP-even mass squared matrix $M_{\text{CP-even}}^2$ can be diagonalised using the orthogonal matrix \mathcal{R} as:

$$\mathcal{R} M_{\text{CP-even}}^2 \mathcal{R}^T = \text{diag}(m_h^2, m_S^2, m_H^2). \quad (16)$$

It is important to note that this model can connect the anomalies and features seen and discussed in section 1, including the few analyses performed in Refs. [8, 10, 11, 18, 19], by considering the couplings of additional bosons among themselves, as well as with gauge bosons and fermions. For example, consider the coupling of $H_i = (h, S, H)$ with a pseudo-scalar A and the Z boson, where the Feynman rule is given by:

$$\lambda_\mu(H_i Z A) = \frac{\sqrt{g^2 + g'^2}}{2} (p_{H_i} - p_A)_\mu \tilde{c}(H_i Z A), \quad (17)$$

where g' is the $U(1)_Y$ gauge coupling with $\tilde{c}(hZA) = -c_{\alpha_2} s_{\beta-\alpha_1}$, $\tilde{c}(SZA) = s_{\beta-\alpha_1} s_{\alpha_2} s_{\alpha_3} + c_{\alpha_3} c_{\beta-\alpha_1}$, and $\tilde{c}(HZA) = c_{\alpha_3} s_{\beta-\alpha_1} s_{\alpha_2} - s_{\alpha_3} c_{\beta-\alpha_1}$. The four-momenta p_{H_i} and p_A of H and A respectively, are taken as incoming. It is to be noted that the tilde over the coupling factor (\tilde{c}) denotes that it is not an effective coupling, since due to no SM counterpart it is not normalised to a corresponding SM coupling. Similarly, the trilinear Higgs coupling hSH is given by:

$$\begin{aligned} \lambda_{hSH} = \frac{1}{v} \bigg(& \mu^2 \left[(2\mathcal{R}_{12}\mathcal{R}_{13} + \mathcal{R}_{32}\mathcal{R}_{33})c_\beta + (\mathcal{R}_{31}\mathcal{R}_{33} - 3\mathcal{R}_{12}\mathcal{R}_{23}\mathcal{R}_{33} - \mathcal{R}_{21}\mathcal{R}_{23})s_\beta \right. \\ & \left. + 3\mathcal{R}_{12}\mathcal{R}_{22} \left(\frac{\mathcal{R}_{31}}{c_\beta} - \frac{\mathcal{R}_{32}}{s_\beta} \right) + 3\mathcal{R}_{13}\mathcal{R}_{23}\mathcal{R}_{31} \frac{s_\beta^2}{c_\beta} \right] \\ & \left. + \frac{\sum_{i=1}^3 m_{H_i}^2}{v_S} \left[\mathcal{R}_{13}\mathcal{R}_{23}\mathcal{R}_{33}v + \mathcal{R}_{12}\mathcal{R}_{22}\mathcal{R}_{32} \frac{v_S}{s_\beta} - \mathcal{R}_{11}(\mathcal{R}_{22}\mathcal{R}_{32} + \mathcal{R}_{23}\mathcal{R}_{33}) \frac{v_S}{c_\beta} \right] \right), \end{aligned} \quad (18)$$

where $\mu^2 = m_{12}^2/(s_\beta c_\beta)$ and \mathcal{R}_{ij} are the elements of the orthogonal matrix \mathcal{R} . In this model the Yukawa Lagrangian is given as:

$$\mathcal{L}_Y = - \sum_{i=1}^3 \frac{m_f}{v} c(H_i f f) \bar{\psi}_f \psi_f H_i, \quad (19)$$

where the coupling coefficient $c(H_i f f)$ are shown in Table 1 in terms of mixing matrix elements \mathcal{R}_{ij} and mixing angle β and the couplings of A and H^\pm are same as in the 2HDMs. For further details we refer the reader to Ref. [28].

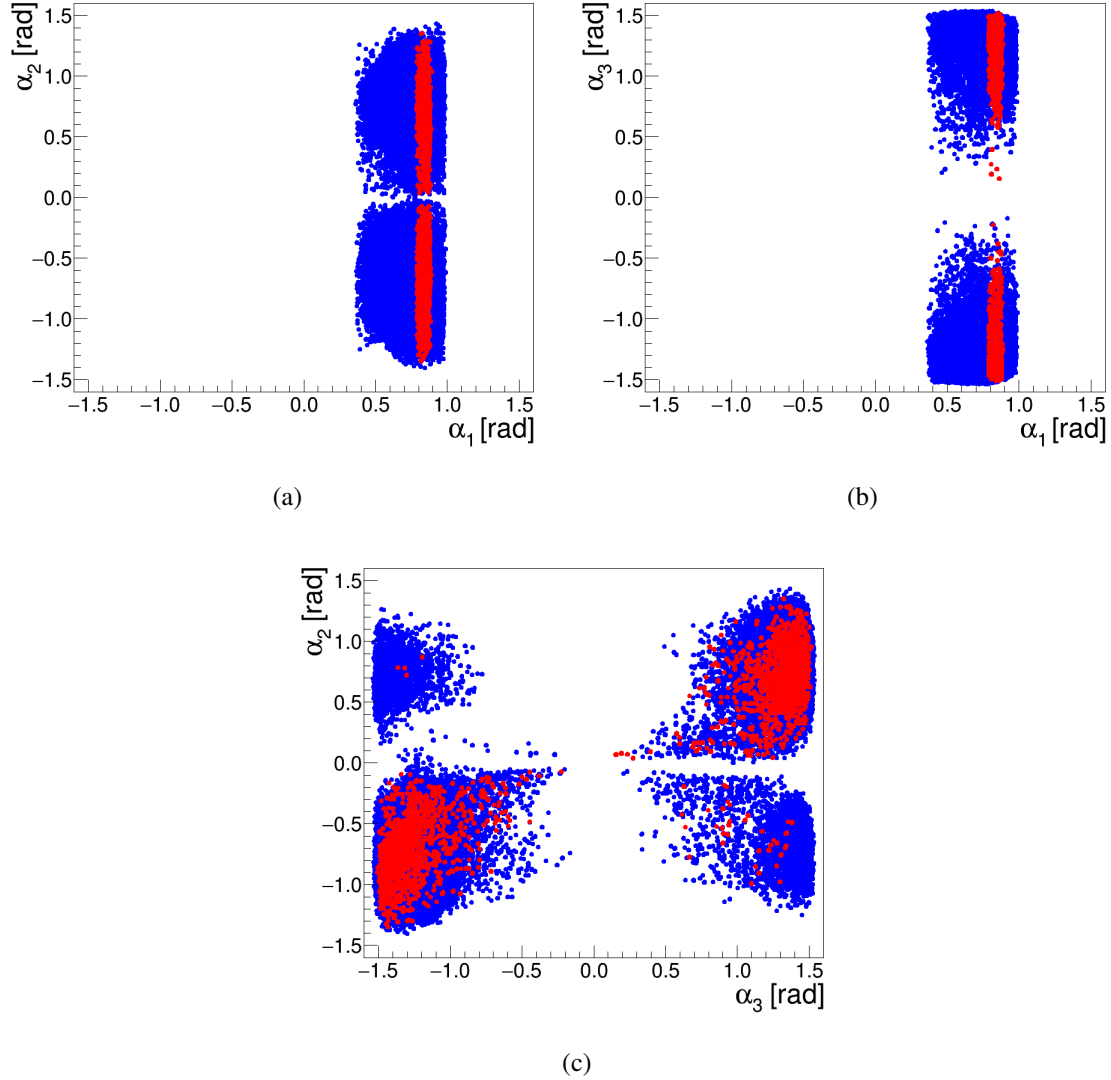


Figure 1. Allowed values of α_1, α_2 and α_3 for the benchmark considered here, where the values in red (blue) are by considering the BRs of the lightest CP-even scalar consistent within 10% (20%) of the prediction for the SM Higgs boson.

It is also important to note that the parameter space described in Ref. [28] and the one chosen for this work (see next section 3) are checked with respect to: (a) theoretical constraints, like tree-level perturbative unitarity, the vacuum stability from global minimum conditions of the 2HDM+S potential and conditions which bound the potential from below; (b) the experimental constraints from R_b [32, 33] and $B \rightarrow X_s \gamma$ [33–36]; and (c) the compatibility with the oblique parameters S, T and U .

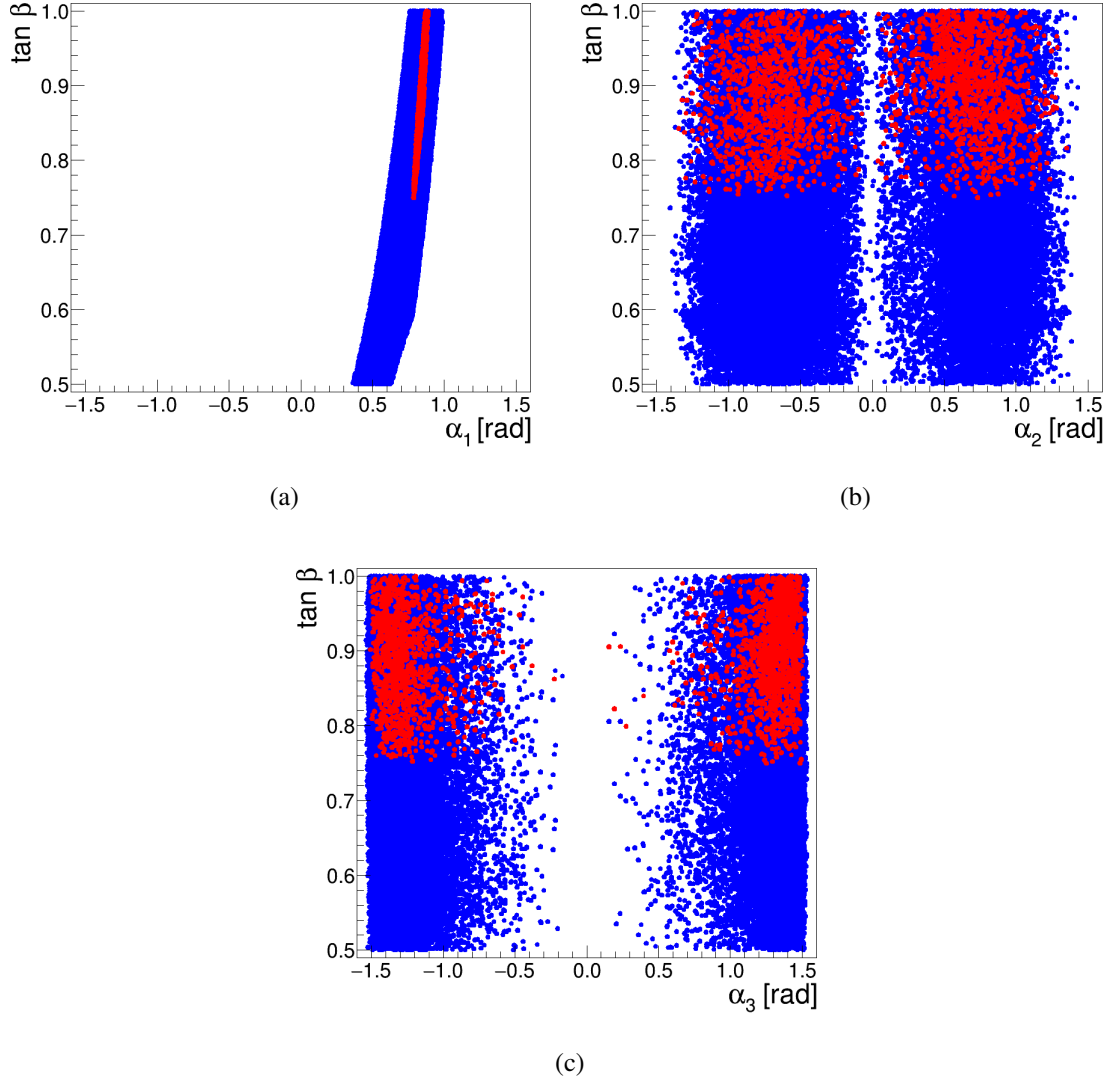


Figure 2. Allowed values of α_1, α_2 and α_3 against $\tan\beta$ for the benchmark considered here, where the values in *red* (*blue*) are by considering the BRs of the lightest CP-even scalar consistent within 10% (20%) of the prediction for the SM Higgs boson.

3. Tools and phenomenology

In the 2HDM+S model described in section 2, the input parameters are following:

$$\alpha_1, \alpha_2, \alpha_3, \tan\beta, v, v_S, m_{H_{1,2,3}}, m_A, m_{H^\pm}, m_{12}^2. \quad (20)$$

For our phenomenological analysis we use type-II 2HDM+S throughout and fix the masses of CP-even and CP-odd scalars in the theory as a benchmark point. From here we denote the lightest CP-even scalar as around the SM Higgs boson with mass $m_h = 125$ GeV, the second one as S with mass $m_S = 140$ GeV, and the heaviest one as H with mass $m_H = 270$ GeV. The CP-odd neutral scalar mass $m_A = 600$ GeV and the charged scalar is taken with $m_{H^\pm} = 600$ GeV. These mass values of the scalars are based on the previous studies considered by the

authors of Ref. [10]. Other parameters are varied in different ranges $-\pi/2 \leq \alpha_{1,2,3} \leq \pi/2$, $0.5 \leq \tan\beta \leq 1.0$. Further, we also vary the masses of scalars, v_S , m_{12}^2 for relevant studies and mentioned at appropriate sections. For numerical calculations we use the publicly available code N2HDECAY [28]. The N2HDECAY code calculates all 2HDM+S scalar boson decay widths and branching ratios (BRs), which include higher order QCD corrections and off-shell decays, however, in this code electroweak corrections are neglected. Furthermore, theoretical constraints on this model for the above-defined benchmark points, like perturbative unitarity and vacuum stability, are also checked with the package ScannerS [37].¶ In addition to these, the following constraints are applied to get the allowed parameter space:

- BRs of the lightest boson should be consistent with the SM within 20% and 10%. This is in order to comply with the wealth of constraints coming from the SM Higgs boson measurements.
- The sum of the BRs of the heavy scalar to lighter scalars should be 80%-90% [1].
- The size of the coupling of h to particles in the SM must be in the range 0.8 ± 0.12 of the prediction of the SM [38].
- Based on the estimate of the Yukawa coupling of the heavy scalar to top quarks, $\beta_g^2 = 1.38 \pm 0.22$ [1], where β_g is a scaling factor with respect to the SM. From here it follows $\tan^2\beta = 0.72 \pm 0.12$.

In Figure 1 we show the allowed values of α_1 , α_2 and α_3 for the benchmark considered here. One can appreciate that the mixing angle α_1 seems more constrained than the other mixing angles. The constraints on α_2 and α_3 are better appreciated in Figure 1 (c), where one can see that certain areas in the plane are excluded. Results are shown by imposing the condition that the BRs of the lightest scalar be consistent within 20% and 10%. Going from 20% to 10% has a strong impact on how the mixing angles are constrained. Figure 2 displays the correlation between mixing angles and $\tan\beta$, where the results are also shown for the two different constraints on the BRs of the light scalar. The allowed values of $\tan\beta$ become more constrained while going from 20% to 10%. The correlation between $\tan\beta$ and α_1 is noticeable, while the correlation with α_2 and α_3 appears small.

Currently, the sensitivity to the Higgs boson BRs at the LHC is not significantly better than 20%. This leaves a significant window of opportunity for new physics. Here we investigate the correlations among the relevant BRs that emerge within this 20% constraint, where ratios of BRs can vary considerably. In Figure 3 we show these correlations for a 20% as well as for 10%. One can appreciate that the allowed parameter space corresponding to a maximum 10% deviation is considerably more constrained than for 20%. This has to do with the fact that the central values for some of the BRs deviate from the SM, thus strongly restricting the range of deviations from the SM. As the values of the BR departure form the central values of the SM, the blue bands become narrower. While the decay $h \rightarrow Z\gamma$ is not yet observed at the LHC, the correlation between the $h \rightarrow WW$, $h \rightarrow \gamma\gamma$ and $h \rightarrow b\bar{b}$ rates can now be measured by the experiments. The ratio of the BR of $h \rightarrow WW$ to that of $h \rightarrow \gamma\gamma$ will

¶ This package is used to perform the checks described in section 2 and Ref. [28] in addition with bounds from the collider searches at Tevatron, LEP and LHC.

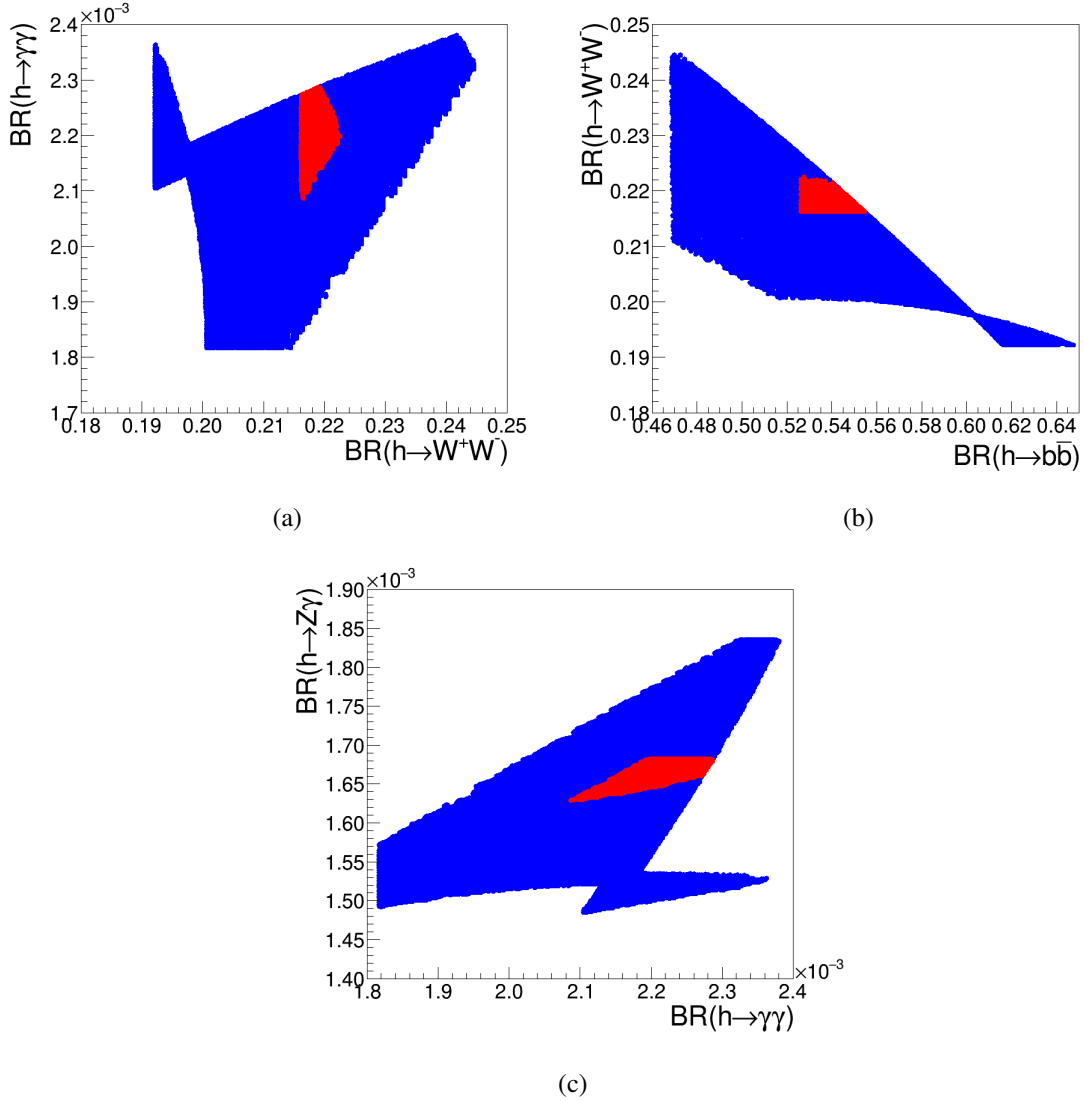


Figure 3. Correlation plots between the BRs of (a) $h \rightarrow WW$ vs $h \rightarrow \gamma\gamma$, (b) $h \rightarrow b\bar{b}$ vs $h \rightarrow WW$ and (c) $h \rightarrow \gamma\gamma$ vs $h \rightarrow Z\gamma$ where the values in red (blue) are by considering the BRs of the lightest h boson consistent within 10% (20%).

be measured with an accuracy better than 3%, and an integrated luminosity that is expected to be accumulated by the High Luminosity LHC. This can be achieved with the application of a full jet veto, where theoretical uncertainties corresponding to the signal production will cancel.

Figure 4 displays the correlations between the BRs of S to SM particles. As opposed to the SM Higgs boson, S is significantly less constrained. Three distinct regimes can be appreciated in Figure 4 (b). The first regime corresponds to the dominance of the $S \rightarrow b\bar{b}$ decay, where the second corresponds to the dominance of the $S \rightarrow WW$ decay for $m_S = 140$ GeV. The latter regime would be the preferred one in light of the multi-lepton excesses reported in Ref. [1]. This behaviour is closer to that displayed by a SM Higgs-like boson. In section 4 S will be assumed to have the same decays as the SM Higgs boson

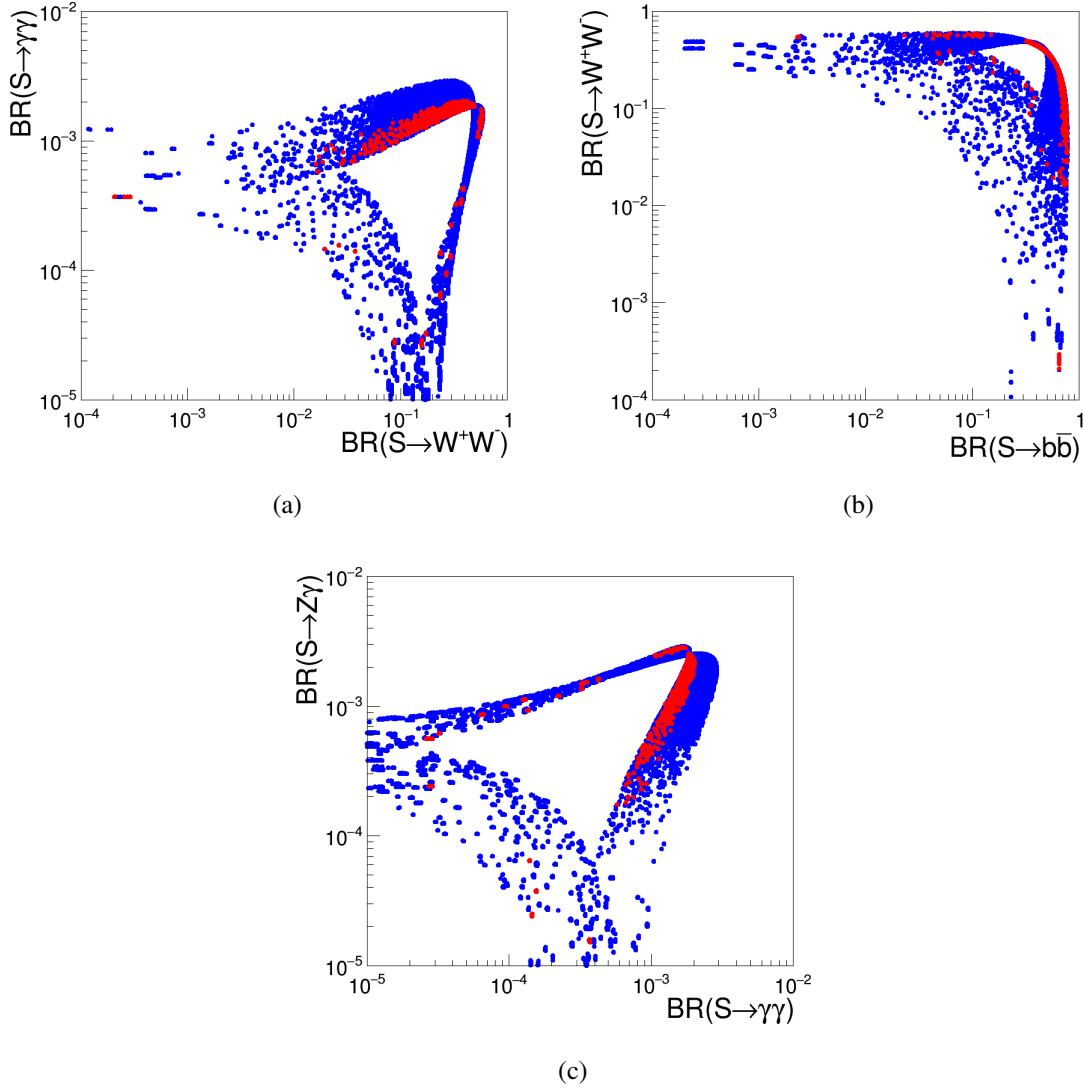


Figure 4. Correlation plots between the BRs of (a) $S \rightarrow WW$ vs $S \rightarrow \gamma\gamma$, (b) $S \rightarrow b\bar{b}$ vs $S \rightarrow WW$ and (c) $S \rightarrow \gamma\gamma$ vs $S \rightarrow Z\gamma$ where the values in red (blue) are by considering the BRs of the lightest h boson consistent within 10% (20%). Here $m_S = 140$ GeV and $m_H = 270$ GeV.

after taking m_S into account.

The two regimes identified here generate certain correlations in the $\text{BR}(S \rightarrow \gamma\gamma)$ vs $\text{BR}(S \rightarrow WW)$ plane, shown in Figure 4 (a), and the $\text{BR}(S \rightarrow Z\gamma)$ vs $\text{BR}(S \rightarrow \gamma\gamma)$ plane, shown in Figure 4 (c). The first regime corresponds to the ridges in Figure 4 (a) and (c) where the $\text{BR}(S \rightarrow \gamma\gamma)$ is largest. The second and preferred regime corresponds to a situation where $\text{BR}(S \rightarrow Z\gamma) > \text{BR}(S \rightarrow \gamma\gamma)$, with $\text{BR}(S \rightarrow Z\gamma) \approx 10^{-3}$. The latter can be accessible at the High Luminosity LHC [39].

There is a third regime where both BRs in Figure 4 (b) display moderate values. In this regime $\text{BR}(S \rightarrow Z\gamma)$ and $\text{BR}(S \rightarrow \gamma\gamma)$ are small and of order of 10^{-4} .

Furthermore, we investigate the BRs of S, H, A and H^\pm to understand the implications of the constraints detailed above on the decays, and how these can lead to final states that

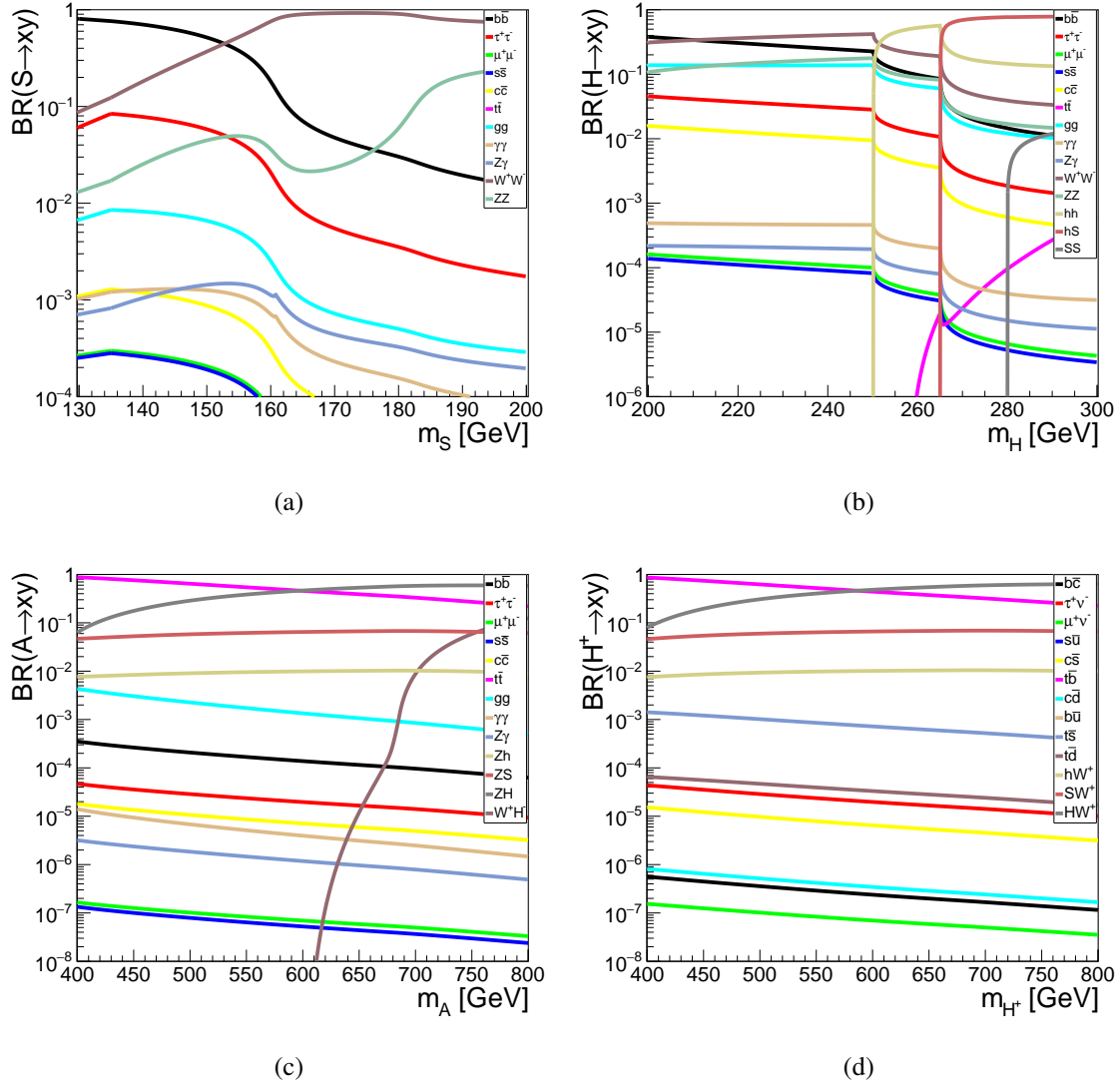


Figure 5. (a) Plot of $BR(S \rightarrow xy)$ against m_S , (b) $BR(H \rightarrow xy)$ against m_H . (c) $BR(A \rightarrow xy)$ against m_A and (d) $BR(H^\pm \rightarrow xy)$ against m_{H^\pm} on the right. In the left, it is shown that the CP-odd scalar A decays predominantly to ZH if its mass is above 600 GeV. On the right, the charged scalar H^\pm decays predominantly to HW^\pm if its mass is greater than 600 GeV.

have not been explored before in the context of searches for new bosons. For this purpose a set of allowed parameter values is selected: $\alpha_1 = +0.885$, $\alpha_2 = -0.167$, $\alpha_3 = -1.28$, $m_{12}^2 = 3.5 (\text{TeV})^2$ and $v_S = 1.5 \text{ TeV}$. Figure 5 shows the BRs of S, H, A and H^\pm in the mass ranges (130 - 200), (200 - 300), (400 - 800) and (400 - 800) GeV, respectively. This benchmark ensures that the experimental constraints detailed above are described by the model.

Figure 5 (a) displays the BRs of the S boson to SM particles, where the mass of S is varied within (130 - 200) GeV [10]. One can appreciate that the selected set of parameters sit within the regime where the decay to $b\bar{b}$ is dominant for $m_S = 140 \text{ GeV}$ (see the earlier discussions regarding Figure 4). For the case when S is treated as a SM Higgs-like boson, the BRs to W^+W^- and $b\bar{b}$ cross just above $m_S = 130 \text{ GeV}$, where here it happens just over 150 GeV. On

the other hand, the BRs of $Z\gamma$ and $\gamma\gamma$ in the SM Higgs-like boson case crosses at 130 GeV, but here this happens at 145 GeV. In the case of $\tau^+\tau^-$ and ZZ^* the corresponding masses are 130 GeV and just over 150 GeV, respectively. In this setup the decay to $b\bar{b}$ is dominant up to $m_S = 155$ GeV above which the decay to W^+W^- becomes dominant.

Figure 5 (b) displays the BRs of the H boson. It is shown that the CP-even heavy scalar H decays predominantly to hh for $250 < m_H < 265$ GeV while above $m_H = 265$ GeV the $H \rightarrow Sh$ BR is dominant. These limits on the masses depend on the masses of the other scalars and it is due to the fact that the N2HDECAY program does not include Higgs-to-Higgs off-shell decays in computing the BRs. In this setup, and ignoring off-shell decays involving S and h bosons, the dominant decay up to $m_H \approx 200$ GeV is $b\bar{b}$, where the decay to W^+W^- overtakes it at $m_H \approx 210$ GeV. The BRs for rare decays, such as $\gamma\gamma$, $Z\gamma$ and $\mu^+\mu^-$ for $m_H < 2m_h$ are of the order of 10^{-4} . It should be noted that the results from Figures 5 (a) and (b) respect the sum rule, which states that the coupling squared of the CP-even scalars to VV ($V = W^\pm, Z$) have to add up to 1 in terms of the squared SM Higgs coupling to VV .

The constraints from the data implemented here apply to the masses and production rates of the neutral scalar bosons. It is therefore very interesting to evaluate the impact on the BRs of the pseudo-scalar and the charged scalar with the assumption that $m_A, m_{H^\pm} > m_H$. Figure 5 (c) displays the BRs of the pseudo-scalar. With the parameter choice used here the dominant decay mode in the range $2m_t < m_A < 600$ GeV is $A \rightarrow t\bar{t}$. For $m_A > 600$ GeV the dominant decay is $A \rightarrow ZH$. The latter leads to interesting final states, as discussed in Ref. [10]. In section 4 we further investigate this decay and, most notably, we scrutinise the rate of production of ZH in association with b -tagged jets. In addition, the production of Z in association with a lepton and b -tagged jets coming from this decay is compared to the data reported by CMS. The production of this final state with a large enough rate to be produced at the LHC is a feature of the $A \rightarrow ZH$ decay. The third most important decay is $A \rightarrow ZS$, which also leads to interesting final states [10]. The decay $A \rightarrow Zh$ is suppressed and sits at the level of 1%. The production of Zh in association with S and h would come from the decay chain $A \rightarrow ZH \rightarrow ZSh, Zh h$ (see Figure 5 (b) and section 4). As the pseudo-scalar gets heavier the decay $A \rightarrow W^\pm H^\mp$ opens up. A distinctive feature of this model is that the decay $A \rightarrow \tau^+\tau^-$ would be suppressed, sitting at the level of $10^{-4} - 10^{-5}$, depending on the mass and same follows for the decay $A \rightarrow b\bar{b}$ with a factor of ~ 10 larger.

Figure 5 (d) shows the BRs of the charged scalar. The decay $H^+ \rightarrow t\bar{b}$ is dominant up to $m_{H^+} \approx 600$ GeV, where the $H^+ \rightarrow HW^+$ decay becomes dominant. The latter leads to a tri-boson final state following $H \rightarrow hS, hh, W^+W^-, ZZ$ at tree-level. The production of charged Higgs bosons can occur via different modes, $gg, q\bar{q}$ fusion in association with t - and b -quark at the LHC. Also H^\pm can be produced in association with t -quark through the mechanism $gb \rightarrow tH^\pm$. Henceforth, multiple leptons in association with b -tagged jets are expected in these production and decay modes of charged Higgs bosons [10]. The third dominant decay is $H^+ \rightarrow SW^+$, where as in the case of the $A \rightarrow \tau^+\tau^-$, the $H^+ \rightarrow \tau^+\nu$ decay is suppressed. The decay $H^+ \rightarrow hW^+$ is suppressed relative to the $H^+ \rightarrow HW^+, SW^+$ decays and it stands at about 1%.

Production cross-sections of different bosons have been checked with the set of

parameters used here. The production cross-section of the scalar S is about ten times smaller than that of the SM Higgs boson. The cross-section for the production of H is compatible with that obtained in Ref. [1]. Therefore, the main production mechanism for S would be that of the decay of H .

4. Comparisons to data

The primary aim of this section is to confront the data with the benchmark points in the parameter space described in section 3. One of the relevant implications with regards to heavy pseudo-scalars considered here is the dominance of $A \rightarrow t\bar{t}, ZH$ decays, where the decay $A \rightarrow Zh$ appears suppressed. As seen in Figure 5, the branching ratio of the $A \rightarrow ZH$ decay becomes dominant for $m_A > 600$ GeV. The decay $A \rightarrow ZH$ leads to interesting final states, as pointed out in Ref. [10]. For the sake of simplicity, here we consider the case where S decays exclusively to SM particles and the decays $H \rightarrow hh, Sh$ are dominant.

It is important to reiterate that the scan performed in this section pertains to a significant number of measurements that do not include the $A \rightarrow Zh$ resonance search, which is interpreted here as emerging from $A \rightarrow ZH \rightarrow hh, Sh$. Therefore, the parameters are greatly constrained by data different from the Zh spectrum. The latter constrains the mass of the pseudo-scalar, whereas the branching ratios are constrained with other data sets.

A distinctive set of final states that emerge from the $A \rightarrow ZH$ decay is the production of relatively high transverse momentum Z bosons in association with a lepton and two b -tagged jets. This final state would not appear in $A \rightarrow Zh$ decay in that no additional leptons would be expected in addition to the Z boson and b -tagged jets. The $bbA(\rightarrow Zh)$ production mechanism could produce this final state. However, the yield would be too small, as discussed below. The CMS experiment has recently reported a discrepancy in the production of Z bosons with an additional lepton, b -tagged jets and low additional jet multiplicity [26, 27]. The discrepancy, corresponding to a local significance of 2.85σ , appears in the study of the production of $t\bar{t}Z$ with $Z \rightarrow \ell\ell, \ell = e, \mu$. Here we interpret this discrepancy with the production of $A \rightarrow ZH$, where the parameters of the model are fixed elsewhere, as discussed above.

Monte Carlo simulation samples are used to model the background and signal processes for this search. Signal samples are simulated using PYTHIA8 [40] and then passed through DELPHES [41] to estimate the detector response. Events were generated for an A boson mass at fixed working points: 500, 550 and 600 GeV. For the interpretation of the $H \rightarrow Sh$, where h is the Higgs boson with $m_h=125$ GeV, the masses of the H and S are assumed to be equal to 270 GeV and 145 GeV, respectively. For simplicity, S BRs are taken from that of the SM Higgs boson at the corresponding mass. Jets were clustered using FAST-JET [42] with the anti- k_T algorithm [43] using the distance parameter, $R = 0.4$.

Section 4.1 covers the interpretation of the $A \rightarrow Zh$ search, whereas section 4.2 interprets the discrepancy observed in the $Z(\rightarrow \ell\ell) + \ell + 2b$ -tagged jet final state.

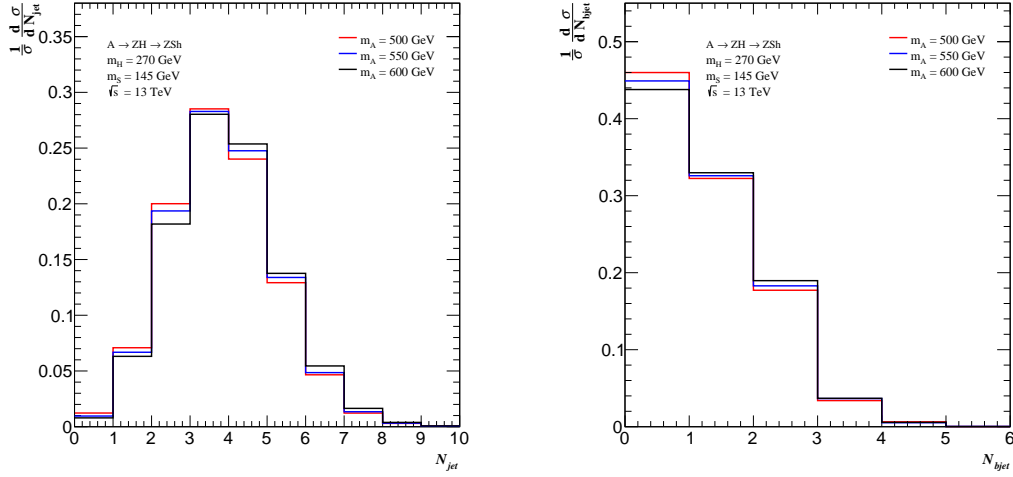


Figure 6. The jet multiplicity for the decay $A \rightarrow ZH \rightarrow ZSh$ produced via gluon-gluon fusion (see text). The plot on the left corresponds to all jets, whereas the plot on the right shows the multiplicity of b -tagged jets.

4.1. $A \rightarrow Zh$ search

The ATLAS and CMS collaborations perform searches for a CP-odd heavy scalar within a 2HDM using various decay channels, where the decay $\ell\ell b\bar{b}$ plays an important role. A structure in the Zh invariant mass spectrum has been recently reported by the ATLAS collaboration [22] with Run 2 data. The CMS collaboration has reported limits with Run 1 data that do not contradict these results [23].

The authors of Ref. [25] have interpreted the structure in terms of a 2HDM where $A \rightarrow Zh$. Here we attempt a different interpretation in light of the spectroscopy discussed in Refs. [8, 10] and Ref. [1] in the context of an extension of the 2HDM, as discussed in section 2. In Ref. [10] it was demonstrated that the decay chain $A \rightarrow ZH$, where $H \rightarrow Sh$ generates a structure in the invariant mass spectrum of the Zh system that resembles that of a resonance with moderate width and a mass in the neighbourhood of $m_A - m_S$. The structure reported in Ref. [22] peaks around 450 GeV. Assuming $m_S = 145$ GeV, the mass of the pseudo-scalar considered here is 600 GeV. The corresponding cross-section of the structure lies in the range between 100 fb and 300 fb.

An important feature of the Zh structure is that it also appears in events with additional b -tagged jets. Within the context of a 2HDM the structure has been interpreted in terms of the ggF and bbA production mechanisms. In the scenario considered here, the decay entails a three boson final state that also produces a structure in the Zh invariant mass spectrum in association with additional b -tagged jets.

Figure 6 displays the multiplicity of all jets and b -tagged jets for the decay $A \rightarrow ZH \rightarrow ZSh$ produced via ggF. Hadronic jets have $p_T > 25$ GeV and $|\eta| < 2.5$. One can appreciate that the average jet multiplicity overshoots that expected from the direct production of $A \rightarrow Zh$. Because of the significant branching ratio of $S \rightarrow b\bar{b}$, the yield of events with more than two

Process	$A(450) \rightarrow Zh$	$bbA(450) \rightarrow bbZh$	$A(600) \rightarrow Zhh$	$A(600) \rightarrow ZSh$
Efficiency	1	1.13	1.23	0.81
$f(N_b = 2)$	0.95	0.83	0.73	0.77
$f(N_b > 2)$	0.05	0.17	0.27	0.23

Table 2. The efficiency of different production mechanisms of Zh after the application of the event selection described in the text with respect to the ggF production of $A \rightarrow Zh$ in a 2HDM. The second and third rows display the fraction of events with exactly two or more than two b -tagged jets after the application of the same event selection. Here $m_H = 270$ GeV and $m_S = 145$ GeV are used, where S is treated as a SM Higgs-like scalar.

b -tagged jets becomes significant so as to mimic the production of bbA in a 2HDM.

In order to evaluate the ability of the 2HDM and the 2HDM+S approaches to describe the data the event selection described in Ref. [22] is adopted here as a baseline. This includes the following requirements:

- At least two b -tagged jets are required such that $p_T > 20$ GeV and $|\eta| < 2.5$. The invariant mass of the two leading b -tagged jet has to lie in the range $100 - 145$ GeV. The transverse momentum of the leading b -tagged jet has to be greater than 45 GeV.
- It is required to have at least two leptons, the transverse momentum of the leading and sub-leading leptons should be greater than 27 GeV and 7 GeV, respectively.
- The missing transverse momentum is required to be below a threshold (in GeV):

$$E_T^{miss}/\sqrt{H_T} < 1.15 + 8 \times 10^{-3} \cdot m_{Zh}, \quad (21)$$

where H_T is defined as the scalar sum of the transverse momenta of all leptons and hadronic jets.

- The transverse momentum of the di-lepton system should conform to the following expression (in GeV):

$$p_T^{\ell\ell} > 20 + 9 \cdot \sqrt{m_{Zh} - 320} \quad (22)$$

This requirement is applied for $m_{Zh} > 320$ GeV.

- The invariant mass of the di-lepton system should obey the following expression (in GeV):

$$\max[40, 87 - 0.030 \cdot m_{Zh}] < m_{\ell\ell} < 97 + 0.013 \cdot m_{Zh} \quad (23)$$

It is probably relevant to note that this event selection is the result of optimizing for the sensitivity of the search for $A \rightarrow Zh$ in a 2HDM. Here the efficiencies for different production mechanism relative to the ggF production of $A \rightarrow Zh$, in a 2HDM are compared. After the application of the requirements described above the relative rate of additional production of b -tagged jets is evaluated.

Table 2 shows the efficiency of the different mechanisms for the production of Zh with respect to the ggF production of $A \rightarrow Zh$ in a 2HDM. The efficiency of $A(600) \rightarrow Zh$ is 23% larger and $A(600) \rightarrow ZSh$ is 19% smaller than that obtained with $A(450) \rightarrow Zh$. The fraction of events with at least one additional b -tagged jet varies

for different production mechanisms. The fraction is small for $A(450) \rightarrow Zh$, whereas for $bbA(450) \rightarrow bbZh$ the fraction increases to 17%. The fraction of events with additional b -tagged jets increases to 27% and 23% for $A(600) \rightarrow ZH \rightarrow Zhh$ and $A(600) \rightarrow ZH \rightarrow ZSh$, respectively. The fraction of events in the Zh mass region between 400 GeV and 500 GeV with an additional b -tagged jet is about 25% of the total amount of events in the structure, but the statistical error on this fraction is too large at this moment.

Appendix 6 provides further details pertaining to the efficiency of $A \rightarrow ZH \rightarrow Zhh$ and $A \rightarrow ZH \rightarrow ZSh$ after the application of cuts used in this section. The final signal efficiency ranges between 0.1% and 0.35%, depending on the pseudo-scalar mass and the decay. Appendix 6 also shows the invariant mass of the Zh system after the application of all cuts. For illustration purposes, for a signal $A(600) \rightarrow ZH \rightarrow ZS(145)h$ and assuming a cross-section of 300 fb and 36 fb^{-1} of integrated luminosity, the signal yield would correspond to about 25 events compared to a background of about 100 events.

4.2. Three leptons in association with two b -tagged jets

The CMS collaboration has reported a discrepancy in a particular corner of the phase space [27]. This includes the presence of two opposite sign and same flavor charged leptons (electrons or muons) with the invariant mass close to that of the Z boson, an additional charged lepton and at least two b -tagged jets. The discrepancy appears in events with exactly two and three hadronic jets. This region of the phase space is weakly populated by the ttZ process, where a large number of hadronic jets is expected. The number of events in the data in excess of the SM prediction corresponds to 28.1 ± 9.5 events with an integrated luminosity of 35.9 fb^{-1} at 13 TeV center of mass energy.

Following Ref. [27], the event selection includes the following kinematic requirements:

- The events are required to have exactly three leptons ($\mu\mu\mu$, $\mu\mu e$, μee or eee), where the leading, subleading, and trailing lepton are required to have p_T thresholds above 40, 20, and 10 GeV, respectively.
- Leptons are required to have $p_T > 10$ GeV and $|\eta| < 2.5$ (2.4) for electrons (muons).
- It is required to have a pair of leptons with an opposite charge and same flavor (OSSF) which satisfies $|m_{\ell\ell} - m_Z| < 10$ GeV.
- Events containing more than one jet are selected, and then are further split into three categories according to the hadronic jet multiplicity, $N_j = 2, 3$, and > 3 .

Hadronic jets, including b -tagged jets, have $p_T > 30$ GeV and $|\eta| < 2.5$. After the application of the event selections described above over the samples we tabulated, the fraction of events for the $A \rightarrow Zhh$ and $A \rightarrow ZSh$ decay channels are as detailed in Table 3. The quantitative analysis reported here indicates that about 60% to 65% of the signal displays low hadronic jet multiplicity with $N_j < 3$.

The efficiency of the event selection with DELPHES is checked against that reported for the production of ttZ in events with at least two b -tagged jets and at more than three jets. Taking into account the results from section 4.1, the expected yield of the signal

Process	N_j	$A = 500 \text{ GeV}$	$m_A = 550 \text{ GeV}$	$m_A = 600 \text{ GeV}$
$A \rightarrow ZH \rightarrow Zhh$	$=2$	0.26	0.27	0.25
	$=3$	0.39	0.38	0.36
	>3	0.35	0.35	0.39
$A \rightarrow ZH \rightarrow ZSh$	$=2$	0.32	0.27	0.23
	$=3$	0.33	0.36	0.30
	>3	0.35	0.37	0.46

Table 3. The fraction of events after the application of the event selections described in the text with respect to three lepton final states for both $A \rightarrow ZH \rightarrow Zhh$ and $A \rightarrow ZH \rightarrow ZSh$ signals. Here $m_H = 270 \text{ GeV}$ and $m_S = 145 \text{ GeV}$ are used.

$A(600) \rightarrow ZH(270) \rightarrow ZS(145)h$ with $N_j < 3$ is about 3 events. This is to be compared to a background of about 50 events. This estimate appears low despite the relatively large uncertainties that characterise the discrepancy discussed here. That being said, it is very important to note that the simplified ansatz that S behaves as a SM Higgs-like boson plays a very important role in the prediction of the cross-section in the corner of the phase-space described here. The assumption made here impacts directly the branching ratio of S decaying into leptons and the jet multiplicity in the final state. The contribution from the $bbA(450)$ signal in this corner of the phase-space is too little to be considered.

4.3. Measurement of Vh production signal strength

The ATLAS [44, 45] and CMS [46, 47] collaborations have independently reported observation of the decay of the decay $h \rightarrow b\bar{b}$. The evidence reported is based on excesses in the data in the search for the SM Higgs boson in association with a Z or a W boson. In doing so the experiments also report the corresponding signal strength of the Vh production mechanism in the SM.

Different event selections are developed depending on the presence of high transverse momentum charged leptons. Here the impact of the different production mechanisms normalised to the size of the structure observed by ATLAS in the Zh spectrum on the measurement of the Vh signal strength in the different final states is discussed here. The potential contamination from the different BSM signal production mechanisms in the phase-space of the measurement of Vh production is evaluated.

Events with two jets tagged as containing b -tagged jets and with either zero, one or two charged leptons (electrons or muons) are selected. The lepton candidates are required to have $p_T > 7 \text{ GeV}$ and $|\eta| < 2.47$ (2.7) for electrons (muons). All events are required to have at least two jets with $p_T > 20 \text{ GeV}$ and $|\eta| < 2.5$, and exactly two with $100 \text{ GeV} \leq m_{bb} \leq 145 \text{ GeV}$ must pass the b -tagging requirement. The p_T of the leading b -tagged jet is required to be above 45 GeV . Events are assigned to zero-, one- and two-lepton channels depending on the number of charged leptons. In the following, the physics objects and the event selection criteria for each channel are described:

Process	$A(450) \rightarrow Zh$	$bbA(450) \rightarrow bbZh$	$A(600) \rightarrow Zhh$	$A(600) \rightarrow ZSh$
$N_\ell=0$	1.12	1.42	0.68	0.42
$N_\ell=1$	0.05	0.06	0.08	0.07
$N_\ell=2$	0.71	0.70	0.67	0.48

Table 4. The potential contamination from the BSM production mechanisms discussed here in the measurement of the signal strength of the Vh , $Z = Z, W$ in the SM. Results are presented in terms of the signal yield with respect to the Vh production in the SM for zero, one and two charged lepton final states (see text). Here $m_H = 270$ GeV and $m_S = 145$ GeV are used.

- The zero-lepton events are required to have $E_T^{\text{miss}} > 150$ GeV. The scalar sum of the transverse momenta of the jets in the event, H_T , is required to be less than 150 GeV. This is to remove a marginal region of phase space in which the trigger efficiency exhibits a small dependence on the jet multiplicity. Also, the following angular selection is applied:
 - $\Delta\phi(\mathbf{b}_1, \mathbf{b}_2) < 140^\circ$,
 - $\Delta\phi(\mathbf{E}_T^{\text{miss}}, \mathbf{bb}) > 120^\circ$,
 - $\min[\Delta\phi(\mathbf{E}_T^{\text{miss}}, \mathbf{jets})] > 30^\circ$,
 where \mathbf{b}_1 and \mathbf{b}_2 are the two b -tagged jets forming the Higgs boson candidates dijet system \mathbf{bb} , and $\mathbf{E}_T^{\text{miss}} > 150$ GeV is the missing transverse momentum which is defined as the negative vector sum of the transverse momenta of electrons, muons and jets.
- In the one-lepton channel events are required to contain exactly one electron with $p_T > 27$ GeV or one muon with $p_T > 25$ GeV. With the electron an additional of $E_T^{\text{miss}} > 30$ GeV is applied.
- In the two-lepton channel events are required to have exactly two leptons of the same flavor with leading lepton $p_T > 27$ GeV. In dimuon events, the two muons are considered to have opposite-sign charges. The invariant mass of the dilepton system must be consistent with the Z boson mass, such that $81 \text{ GeV} < m_{\ell\ell} < 101 \text{ GeV}$.

Events are then categorised into two categories according to jet multiplicity. In the zero- and one-lepton channels events are considered with three or fewer jets. In the two-lepton channel events are considered with higher jet multiplicities which is three or more jets. Furthermore, selections for the reconstructed vector boson's transverse momentum, p_T^V , are applied. This observable corresponds to E_T^{miss} in the zero-lepton channel, to the vectorial sum of $\mathbf{E}_T^{\text{miss}}$ and the charged lepton's transverse momentum in the one- and two-lepton channels. In the zero- and one-lepton channels a single region is defined, with $p_T^V > 150$ GeV. In the 2-lepton channel two regions are considered, $75 \text{ GeV} < p_T^V < 150 \text{ GeV}$ and $p_T^V > 150 \text{ GeV}$. Here yields of the different signals are integrated for $p_T^V > 75 \text{ GeV}$.

Table 4 displays the potential contamination of the BSM signals. Results are shown in terms of the BSM signal yield normalized to the yield of the SM Vh production in the phase-space described here. A cross-section of 200 fb [22] is assumed for all BSM signals reported in Table 4. It is very important to note that a number of more sophisticated techniques have been used by the experiments to extract the SM signal. As a result, the potential contamination reported in Table 4 is an upper bound of the potential contamination. Making a more accurate

estimate of the contamination goes beyond the scope of this paper. The results shown in Table 4 are better suited for a comparative analysis.

One can appreciate that the contamination on the one-lepton final state is quite small, whereas the contamination on the zero-lepton final state is significant, followed by that of the one-lepton final state. The contamination is maximum for the 2HDM signals, where for the bbA production mechanism the contamination would be largest and comparable to the Vh signal in the SM. By contrast, the 2HDM+S signals have a moderate impact on the SM Vh production where the most important decay, $A \rightarrow ZH \rightarrow ZSh$ would have the smallest effect.

5. Summary and Conclusions

In Refs. [8, 10] scalars H and S were introduced via an effective model to explain a number of features in the Run 1 data. These scalars were embedded into a 2HDM+S model in Ref. [10], where it was pointed out that the anomalous production of multiple leptons would be a prominent feature of the model. This hypothesis has been compared to data [1, 20] where large discrepancies between the data and SM MCs are observed that cannot be resolved with available tools. These discrepancies are interpreted using a simplified model where $m_H = 270$ GeV and $m_S = 145$ GeV.

In this paper we attempt to identify the corners of the parameter space in a 2HDM+S model that satisfy the conclusions arrived at in Ref. [1]. The implications on the decays of the heavy pseudo-scalar and charged scalar are discussed. With the parameter choice used here the dominant decay mode in the range $2m_t < m_A < 600$ GeV is $A \rightarrow t\bar{t}$. For $m_A > 600$ GeV the dominant decay is $A \rightarrow ZH$. The third most important decay is $A \rightarrow ZS$, which also leads to interesting final states. The decay $A \rightarrow Zh$ is suppressed and sits at the level of 1%. The production of Zh would come from the decay chain $A \rightarrow ZH \rightarrow ZSh, Zhh$. As the pseudo-scalar gets heavier the decay $A \rightarrow W^\pm H^\mp$ opens up. A distinctive feature of this model is that the decay $A \rightarrow \tau^+ \tau^-$ would be suppressed, sitting at the level of $10^{-4} - 10^{-5}$ depending on the mass. The decay $H^+ \rightarrow t\bar{b}$ is dominant up to $m_{H^+} \approx 600$ GeV where the $H^+ \rightarrow HW^+$ decay becomes dominant. The third dominant decay is $H^+ \rightarrow SW^+$, the $H^+ \rightarrow \tau^+ \nu$ decay is suppressed. The decay $H^+ \rightarrow hW^+$ is suppressed relative to the $H^+ \rightarrow HW^+, SW^+$ decays. The conclusions from these studies further reinforce the relevance of multi-lepton final states in the search for new bosons.

A structure in the Zh invariant mass spectrum has been reported by the ATLAS collaboration [22] with Run 2 data, which appears in association with b -tagged jets, in addition to those assigned to the decay of h . Here we interpret the structure in terms of the 2HDM+S model. The production of Zh with additional b -tagged jets from $A(600) \rightarrow Z(270)H \rightarrow ZS(145)h, Zhh$ is discussed. The fiducial efficiency of this production mechanism is similar to other production mechanisms, like $A(450) \rightarrow Zh$ and $bbA(450) \rightarrow bbZh$. However, one of the features of the 2HDM+S signal considered here is the production of $Z(\rightarrow \ell\ell)$ in association with a lepton and two b -tagged jets. The jet activity would be significantly different from that displayed by the production of ttZ . An excess is seen by CMS in this final state in events with low additional jet multiplicity, a regime where the production of ttZ is suppressed.

By contrast, the 2HDM signals considered here do not contribute significantly to this final state. The potential existence of a heavy pseudo-scalar would contribute to the production of Zh and contaminate the phase-space where the signal strength of the Vh production is measured by the experiments. The 2HDM signals considered here would bring considerable contamination, where the largest contamination would come from $bbA(450) \rightarrow bbZh$, the preferred option in a 2HDM to explain the structure in the Zh invariant mass spectrum. The preferred signal in a 2HDM+S would yield a moderate impact on the measurement of the Vh signal strength. On the other hand, the mass spectrum of this model is computed at tree-level only though the decays are computed with higher-order corrections. So a non-negligible contribution from one-loop corrections to scalars mass may impact the analyses carried here, for example the observables for $A \rightarrow ZH$ might get affected. Hence, a future study may be followed considering these corrections.

As this paper was being reviewed, CMS and ATLAS have reported excesses in $t\bar{t}$ and $Zb\bar{b}$ final states [48–50] that can be interpreted with $m_A \approx 600$ GeV and in the range of $\tan\beta$ considered here. In conclusion, the 2HDM+S model with the parameters obtained here is able to accommodate the excesses at the LHC reported in Ref. [1]. Without varying these parameters additional excesses in the Zh spectrum and the production of 3 leptons plus two b -tagged jets can be explained assuming $m_A \approx 600$ GeV.

6. Appendix

This appendix reports additional material that is directly relevant to section 4.1. This includes an account of the BSM signal efficiency as a function of the pseudo-scalar mass against the event selection used in section 4.1. Tables 5 and 6 display the BSM signal efficiency after successive event selection requirements for the $A \rightarrow ZH \rightarrow Zhh$ and $A \rightarrow ZH \rightarrow ZSh$ decays, respectively, where $m_H = 270$ GeV and $m_S = 145$ GeV. Results are shown for final states with at least and exactly two b -tagged jets, as detailed in section 4.1. The signal efficiency increases strongly with the pseudo-scalar mass. This driven to a large extent by the requirement in expression (22), which was implemented as a result of an optimization for the 2HDM signal discussed in section 4.1. As a result, the signal efficiency for $m_A = 600$ GeV is about 80% larger than that for $m_A = 500$ GeV. The signal efficiency for the $A \rightarrow ZH \rightarrow Zhh$ decay is superior to that of $A \rightarrow ZH \rightarrow ZSh$ for the choice of masses used here. The final signal efficiency ranges between 0.1% and 0.35%, depending on the pseudo-scalar mass and the decay chain.

Figure 7 displays the distribution of the invariant mass of the Zh system from the $A \rightarrow ZH \rightarrow Zhh$ and $A \rightarrow ZH \rightarrow ZSh$ decays after the application of the event selection detailed in section 4.1. The distributions display a cut-off at 320 GeV described in section 4.1. As the m_A becomes larger so that the phase-space available enhancing the invariant mass of the Zh system and its apparent width.

Constraints on a 2HDM with a singlet scalar and implications in the search for heavy bosons at the LHC22

Cuts	Categories	(I) At least 2 b -jets			(II) Exactly 2 b -jets		
		$m_A = 500$ GeV	$m_A = 550$ GeV	$m_A = 600$ GeV	$m_A = 500$ GeV	$m_A = 550$ GeV	$m_A = 600$ GeV
$N_{bjet} = \text{(I) or (II)}$		0.4454	0.4504	0.4525	0.2871	0.2893	0.2904
Two leptons		0.0127	0.0143	0.0151	0.0097	0.0108	0.0115
$100 < m_{bb}[\text{GeV}] < 145$		0.0052	0.0055	0.0056	0.0041	0.0043	0.0044
$P_T^{led-bj} > 45$ GeV		0.0049	0.0053	0.0054	0.0038	0.0041	0.0042
$P_T^{\ell\ell} > 20 + 9 \cdot \sqrt{m_{Zh} - 320}$ GeV		0.0023	0.0036	0.0041	0.0017	0.0026	0.0030
$\max[40, 87 - 0.030 \cdot m_{Zh}] \leq m_{\ell\ell}[\text{GeV}] \leq 97 + 0.013 \cdot m_{Zh}$		0.0021	0.0035	0.0036	0.0015	0.0023	0.0027
$E_T^{miss} / \sqrt{H_T} < 1.15 + 08 \cdot m_{Vh} [\text{GeV}]$		0.0020	0.0031	0.0035	0.0014	0.0022	0.0025
$A \rightarrow ZH \rightarrow Zh h$							

Table 5. The fraction of events after the application of the event selections described in section 4.1 with respect to at least and exactly two b -tagged jets final states for the signal sample $A \rightarrow ZH \rightarrow Zh h$, with $m_H = 270$ GeV.

Cuts	Categories	(I) At least 2 b -jets			(II) Exactly 2 b -jets		
		$m_A = 500$ GeV	$m_A = 550$ GeV	$m_A = 600$ GeV	$m_A = 500$ GeV	$m_A = 550$ GeV	$m_A = 600$ GeV
$N_{bjet} = \text{(I) or (II)}$		0.3524	0.3587	0.3600	0.2467	0.2493	0.2504
Two leptons		0.0113	0.0122	0.0130	0.0092	0.0100	0.0106
$100 < m_{bb}[\text{GeV}] < 145$		0.0045	0.0046	0.0047	0.0037	0.0038	0.0039
$P_T^{led-bjet} > 45$ GeV		0.0042	0.0043	0.0044	0.0034	0.0036	0.0037
$P_T^{\ell\ell} > 20 + 9 \cdot \sqrt{m_{Zh} - 320}$ GeV		0.0016	0.0026	0.0029	0.0012	0.0020	0.0024
$\max[40, 87 - 0.030 \cdot m_{Zh}] \leq m_{\ell\ell}[\text{GeV}] \leq 97 + 0.013 \cdot m_{Zh}$		0.0014	0.0022	0.0025	0.0010	0.0017	0.0020
$E_T^{miss} / \sqrt{H_T} < 1.15 + 08 \cdot m_{Vh} [\text{GeV}]$		0.0013	0.0021	0.0023	0.0010	0.0016	0.0018
$A \rightarrow ZH \rightarrow ZSh$							

Table 6. The fraction of events after the application of the event selections described in section 4.1 with respect to at least and exactly two b -tagged jets final states for the signal sample $A \rightarrow ZH \rightarrow ZSh$. Here $m_H = 270$ GeV and $m_S = 145$ GeV are used.

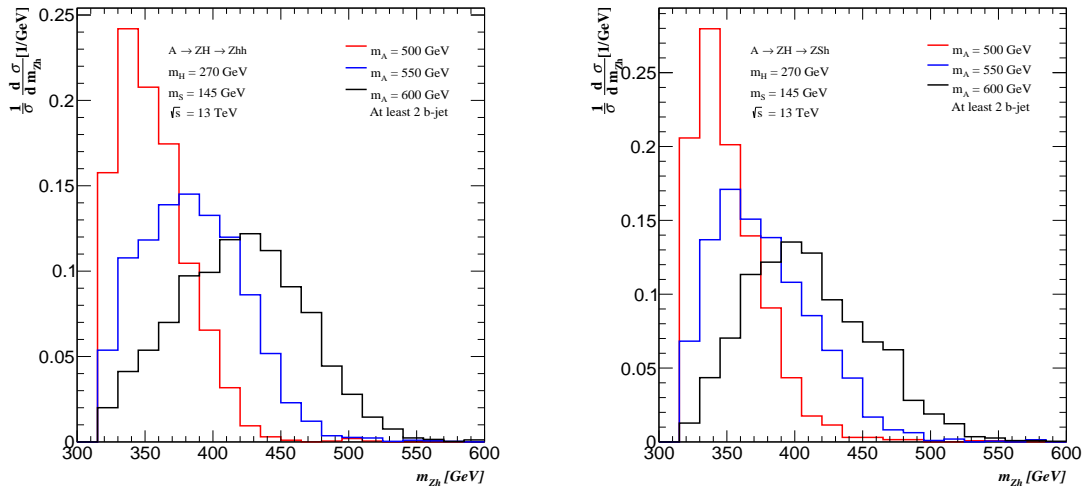


Figure 7. Distribution of the invariant mass of the Zh system from the $A \rightarrow ZH \rightarrow Zh h$ (left) and $A \rightarrow ZH \rightarrow ZSh$ (right) decays, where $m_H = 270$ GeV and $m_S = 145$ GeV. Results are shown for different pseudo-scalar masses after the event selection described in section 4.1.

Acknowledgments

The authors would like to thank the DST for the support through the SA-CERN consortium and the NRF for different types of support. The authors would also like to acknowledge the support from the Research Office of the University of the Witwatersrand. E. Iarilala acknowledges the support from the DAAD program. E. Shrif acknowledges the support from the Faculty for the Future Schlumberger Foundation. The authors would like to thank Toby Opferkuch for assistance with the model files.

References

- [1]S. von Buddenbrock, A. S. Cornell, A. Fadol, M. Kumar, B. Mellado and X. Ruan, J. Phys. G **45**, no. 11, 115003 (2018) [arXiv:1711.07874 [hep-ph]].
- [2]F. Englert and R. Brout, Phys. Rev. Lett. **13** (1964) 321.
- [3]P. W. Higgs, Phys. Rev. Lett. **13** (1964) 508.
- [4]P. W. Higgs, Phys. Lett. **12** (1964) 132.
- [5]G. S. Guralnik, C. R. Hagen and T. W. B. Kibble, Phys. Rev. Lett. **13** (1964) 585.
- [6]G. Aad *et al.* [ATLAS Collaboration], Phys. Lett. B **716** (2012) 1.
- [7]S. Chatrchyan *et al.* [CMS Collaboration], Phys. Lett. B **716** (2012) 30.
- [8]S. von Buddenbrock *et al.*, arXiv:1506.00612 [hep-ph].
- [9]M. Kumar *et al.*, J. Phys. Conf. Ser. **802**, no. 1, 012007 (2017) [arXiv:1603.01208 [hep-ph]].
- [10]S. von Buddenbrock *et al.*, Eur. Phys. J. C **76**, no. 10, 580 (2016) [arXiv:1606.01674 [hep-ph]].
- [11]Y. Fang, M. Kumar, B. Mellado, Y. Zhang and M. Zhu, Int. J. Mod. Phys. A **32** (2017) no.34, 1746010 [arXiv:1706.06659 [hep-ph]].
- [12]C. Mosomane, M. Kumar, A. S. Cornell and B. Mellado, J. Phys. Conf. Ser. **889**, no. 1, 012004 (2017) [arXiv:1707.05997 [hep-ph]].
- [13]L. Delle Rose, O. Fischer and A. Hammad, arXiv:1809.04321 [hep-ph].
- [14]S. P. Das, J. Hernandez-Sanchez, S. Moretti and A. Rosado, arXiv:1806.08361 [hep-ph].
- [15]T. D. Lee, Phys. Rev. D **8**, 1226 (1973).
- [16]G. C. Branco, P. M. Ferreira, L. Lavoura, M. N. Rebelo, M. Sher and J. P. Silva, Phys. Rept. **516**, 1 (2012) [arXiv:1106.0034 [hep-ph]].
- [17]M. Mhlleitner, M. O. P. Sampaio, R. Santos and J. Wittbrodt, JHEP **1708**, 132 (2017) [arXiv:1703.07750 [hep-ph]].
- [18]S. von Buddenbrook, A. S. Cornell, D. Kar, M. Kumar, B. Mellado and R. G. Reed, J. Phys. Conf. Ser. **802**, no. 1, 012001 (2017).
- [19]S. von Buddenbrook, A. S. Cornell, M. Kumar and B. Mellado, J. Phys. Conf. Ser. **889**, no. 1, 012020 (2017) [arXiv:1709.09419 [hep-ph]].
- [20]B. Mellado, Understanding the production of multiple leptons at the LHC, HDAYS2018, Santander, September 10th-14th 2018, <http://hdays.csic.es/HDays18/>.
- [21]S. von Buddenbrook, A. S. Cornell, Y. Fang, A. Fadol Mohammed, M. Kumar, B. Mellado and K. G. Tomiwa, arXiv:1901.05300 [hep-ph].
- [22]M. Aaboud *et al.* [ATLAS Collaboration], JHEP **1803** (2018) 174 [arXiv:1712.06518 [hep-ex]].
- [23]V. Khachatryan *et al.* [CMS Collaboration], Phys. Lett. B **748** (2015) 221 [arXiv:1504.04710 [hep-ex]].
- [24]CMS Collaboration [CMS Collaboration], CMS-PAS-HIG-18-005.
- [25]P. M. Ferreira, S. Liebler and J. Wittbrodt, Phys. Rev. D **97** (2018) no.5, 055008 [arXiv:1711.00024 [hep-ph]].
- [26]A. M. Sirunyan *et al.* [CMS Collaboration], Phys. Rev. D **97** (2018) no.3, 032009 [arXiv:1711.00752 [hep-ex]].
- [27]A. M. Sirunyan *et al.* [CMS Collaboration], JHEP **1808** (2018) 011 [arXiv:1711.02547 [hep-ex]].
- [28]M. Muhlleitner, M. O. P. Sampaio, R. Santos and J. Wittbrodt, JHEP **1703**, 094 (2017) [arXiv:1612.01309 [hep-ph]].
- [29]I. P. Ivanov, Prog. Part. Nucl. Phys. **95**, 160 (2017) [arXiv:1702.03776 [hep-ph]].
- [30]C. Y. Chen, M. Freid and M. Sher, Phys. Rev. D **89**, no. 7, 075009 (2014) [arXiv:1312.3949 [hep-ph]].
- [31]A. Drozd, B. Grzadkowski, J. F. Gunion and Y. Jiang, JHEP **1411**, 105 (2014) [arXiv:1408.2106 [hep-ph]].
- [32]H. E. Haber and H. E. Logan, Phys. Rev. D **62**, 015011 (2000) [hep-ph/9909335].
- [33]O. Deschamps, S. Descotes-Genon, S. Monteil, V. Niess, S. T'Jampens and V. Tisserand, Phys. Rev. D **82**, 073012 (2010) [arXiv:0907.5135 [hep-ph]].
- [34]F. Mahmoudi and O. Stal, Phys. Rev. D **81**, 035016 (2010) [arXiv:0907.1791 [hep-ph]].
- [35]T. Hermann, M. Misiak and M. Steinhauser, JHEP **1211**, 036 (2012) [arXiv:1208.2788 [hep-ph]].
- [36]M. Misiak *et al.*, Phys. Rev. Lett. **114**, no. 22, 221801 (2015) [arXiv:1503.01789 [hep-ph]].

- [37]R. Coimbra, M. O. P. Sampaio and R. Santos, Eur. Phys. J. C **73**, 2428 (2013) [arXiv:1301.2599 [hep-ph]].
- [38]B. Mellado, “The production of additional bosons and the impact on the Large Hadron Collider”, HDAYS, Santander 18th-22th September 2017, <http://hdays.csic.es/HDays17/>.
- [39]G. Aad *et al.* [ATLAS Collaboration], “Update of the prospects for the $H \rightarrow Z\gamma$ search at the High-Luminosity LHC”, ATL-PHYS-PUB-2014-006, <http://cds.cern.ch/record/1703276>.
- [40]T. Sjstrand *et al.*, Comput. Phys. Commun. **191**, 159 (2015) [arXiv:1410.3012 [hep-ph]].
- [41]S. Oryn, X. Rouby and V. Lemaitre, [arXiv:0903.2225 [hep-ph]].
- [42]M. Cacciari, G. P. Salam and G. Soyez, Eur. Phys. J. C **72**, 1896 (2012), [arXiv:1111.6097 [hep-ph]].
- [43]M. Cacciari, G. P. Salam and G. Soyez, JHEP **0804**, 063 (2008), [arXiv:0802.1189 [hep-ph]].
- [44]M. Aaboud *et al.* [ATLAS Collaboration], JHEP **1712** (2017) 024 [arXiv:1708.03299 [hep-ex]].
- [45]The ATLAS collaboration [ATLAS Collaboration], ATLAS-CONF-2018-036.
- [46]A. M. Sirunyan *et al.* [CMS Collaboration], Phys. Lett. B **780** (2018) 501 [arXiv:1709.07497 [hep-ex]].
- [47]CMS Collaboration [CMS Collaboration], CMS-PAS-HIG-18-016.
- [48]A. M. Sirunyan *et al.* [CMS Collaboration], arXiv:1908.01115 [hep-ex].
- [49]CMS Collaboration [CMS Collaboration], CMS-PAS-HIG-18-012.
- [50]M. Aaboud *et al.* [ATLAS Collaboration], Phys. Lett. B **783**, 392 (2018) [arXiv:1804.01126 [hep-ex]].